Polycrystalline Graphene Ribbons as Chemiresistors

Amin Salehi-Khojin, David Estrada, Kevin Y. Lin, Myung-Ho Bae, Feng Xiong, Eric Pop, and Richard I. Masel*

Graphene is a two-dimensional semimetal with zero band gap that exhibits excellent electrical, mechanical and thermal properties.[1,2] Transport through delocalized pi bonds allows charge carriers in graphene to achieve high mobility[3,4] for both electrons and holes, over ~10^5 cm^2/V·s for freely suspended graphene and >10^4 cm^2/V·s for graphene on SiO$_2$.[5] Recent studies have suggested that graphene could also be an interesting chemiresistor material.[6–9] In addition, when functionalized with single-stranded DNA, graphene provides a route towards "sequence-dependent" chemical sensing.[10] Single molecule detection has also been reported[11] using Hall measurements with mechanically exfoliated monolayer graphene. However, prior to this study, the sensitivity of simpler sensing configurations such as two-terminal graphene chemiresistors to many analytes has been below that of chemiresistors based on carbon nanotubes (CNTs).[7–9]

The objective of this work was to understand what limits the sensitivity of simple, two-terminal graphene chemiresistors, and to study this in the context of inexpensive devices easily manufactured by chemical vapor deposition (CVD). We focused on the idea that while graphene shares several similarities with CNTs, graphene is a two-dimensional conductor while CNTs are essentially one-dimensional conductors. Could this difference in dimensionality be responsible for the difference in sensing behavior?

Further, at this point, the physical mechanisms of interaction between adsorbed species and graphene are not as well understood as in CNT sensors. For instance, we have recently shown that point defects in CNTs are key to the highly sensitive response towards target analytes.[12–14] While much of the research within the graphene community is geared towards producing large-scale and defect-free graphene, only recently have linear defects in graphene emerged as a focused area of research.[15–17] The question we then asked is, "Do linear defects enhance the chemical sensitivity in two-dimensional systems such as graphene?"

We produced graphene sensors with both nearly-pristine and deliberately-defective structures. Nearly-pristine sensors were obtained by mechanical exfoliation of monocrystalline graphene, while defective graphene was produced by chemical vapor deposition (CVD) of polycrystalline graphene. Both types of sensors were transferred onto SiO$_2$/Si substrates and contacted by metal electrodes (details are given in the Experimental Section and the Supporting Information). The sensors were exposed to 100 milliseconds of toluene (an electron donor) and to 1,2-dichlorobenzene (an electron acceptor), and the change in the conductance was measured upon exposure to trace gas vapors. Our experiments were designed to compare the response of such graphene chemiresistors made by different procedures, in order to vary the types of defects and determine their role. We note that our four point measurement showed that contact resistance of our sensors is negligible, indicating negligible role of contacts in the sensing mechanism (see Supporting Information for additional information).

We used atomic force microscopy (AFM) and Raman Spectroscopy to characterize defects in our samples (**Figure 1**). No evident defects are found in our "pristine" (exfoliated, monocrystalline) samples by AFM or Raman analysis. However, scanning tunneling microscopy (STM) data of similar samples indicate the presence of a few point defects.[16] By contrast, Figures 1A and 1B show AFM images of "defective" graphene grown by CVD. Our CVD growth process on polycrystalline copper foil yields polycrystalline graphene,[18] where the grain boundaries can act as linear defects.[15,17,19] Transfer processes to remove this polycrystalline graphene from metal growth substrates and place it on insulating substrates also result in wrinkles in the graphene film, which may act as a linear defects.[20] These defects form two different patterns on the graphene surfaces. A few regions of the sample had ~10 μm long well-aligned line defects, like those shown in Figure 1A. However, the majority of the sample had randomly oriented line defects (Figure 1B) with an average length of ~0.7 μm.

Raman spectra of both samples are shown in Figure 1C. The pristine graphene sample does not show a D-peak, suggesting the overall concentration of defects is low and the sample is monocrystalline.[21] By contrast, CVD graphene samples show a large D-peak, from which we can estimate the grain size, L_a (nm) = $2.4 \times 10^{-10} \lambda^4 (I_D/I_G)^{-1}$, where λ is the excitation laser wavelength in nm and (I_D/I_G) is the D-peak to G-peak integrated intensity ratio.[22,23] We find our CVD sample varies between

A. Salehi-Khojin,[+] K. Y. Lin[†]
Department of Chemical and Biomolecular Engineering
University Of Illinois at Urbana Champaign, USA

D. Estrada,[+] M.-H. Bae,[†] F. Xiong,[†] Prof. E. Pop
Department of Electrical and Computer Engineering
University Of Illinois at Urbana Champaign, USA

D. Estrada, M.-H. Bae, F. Xiong, Prof. E. Pop
Micro and Nanotechnology Lab
University Of Illinois at Urbana Champaign, USA

F. Xiong, Prof. E. Pop
Beckman Institute
University Of Illinois at Urbana Champaign, USA

A. Salehi-Khojin Prof. R. I. Masel
Dioxide Materials, 60 Hazelwood Dr, Champaign IL 61820, USA
E-mail: rich.masel@dioxidematerials.com

[+] A.S.-K. and D.E. contributed equally to this work.

[†] K.Y.L., M.-H.B., and F.X. contributed equally to this work.
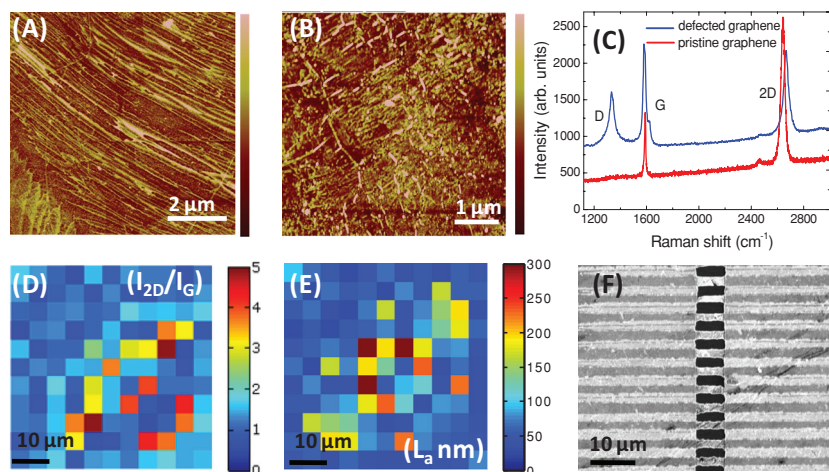
COMMUNICATION

Figure 1. (A and B) AFM images of CVD graphene used for sensors, color scales are 10 and 5 nm, respectively, (C) Raman spectra of pristine and CVD-based "defective" graphene samples, (D) map of I_{2D}/I_G ratio indicating our CVD process produces mono to few layer graphene, (E) map of crystallite size indicative of 30 to >300 nm distance between line defects with an average $L_a \sim 80$ nm (see text), and (F) Scanning electron microscopy image of CVD graphene ribbons.

procedures to eliminate PMMA residues left after the graphene device fabrication for both types of samples, and X-ray photoelectron spectroscopy (XPS) verifies our cleaning procedure removes PMMA (see Supporting Information).[7,25]

We performed an additional experiment to further elucidate the role of line defects on the behavior of our sensors. In this case, we cut the CVD-grown sample into ribbons that were 2 to 5 μm wide, as shown in Figure 1F. By way of background, when a graphene sheet is cut into ribbons with dimensions similar to those of the line defects, edges are created that cross the line defects. Consequently, when an edge crosses a line defect, leakage currents around the sides of the line defect are eliminated. Thus, the edge should enhance the effects of the line defects, provided the length of the line defects is similar to the ribbon width. Point defects should be hardly affected since most of the point defects are far away from the edges. The edges themselves do not affect charge transport significantly, so edges alone should have limited effect on the sensor response; this is the case here because
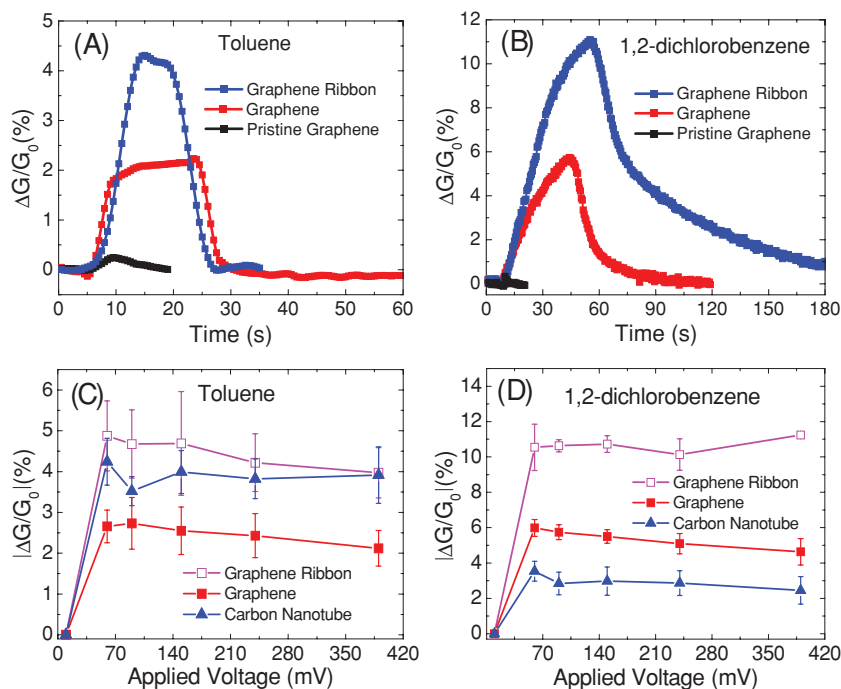
mono and bilayer graphene (Figure 1D), with an average grain size $L_a \sim 80$ nm (Figure 1E). Mobility values for our pristine graphene devices are significantly greater than for devices fabricated from CVD graphene, ≈4.5× (see Supporting Information for additional information). We note that with such a small L_a, the Raman spot size of ≈1 μm samples multiple crystallite domains and that the pixel size of the Raman map (5 μm × 5 μm) does not provide information about the quality of the graphene within a single crystallite. However, this large scale map provides an average value of L_a across an area of graphene comparable to the area of the sensors. Ongoing scanning tunneling microscopy studies of our CVD graphene reveal the regions between the line defects are almost pristine with large perturbations in the material's electronic properties at linear defects. We have not detected many isolated point defects on our CVD graphene samples.[16]

Figures 2A,B compares the response of the two different chemiresistors to a 100 millisecond pulse of toluene (an electron donor) and to 1,2-dichlorobenzene (an electron acceptor). In each case, we chose the number of molecules in the pulse to be similar to the number of molecules produced by our preconcentrator[24] with sampling air containing 300 parts per billion (ppb) of analyte. We find little or no response with the pristine graphene sample, but a large response (up to 50× higher) with the defective and polycrystalline samples. Clearly, the addition of line defects (and perhaps a few point defects) has enhanced the sensor response. We note that we have used well-established cleaning

Figure 2. (A-B) Ratio of conductance to initial conductance (G/G_0) response of CVD-grown defective graphene, CVD graphene microribbon, and 5 μm wide pristine (exfoliated) graphene sensors to 10^{14} molecules of toluene and 10^{15} molecules of 1,2-dichlorobenzene, respectively. The pulses are similar to those produced by a preconcentrator[24] sampling air containing 300 ppb of analyte. (C-D) Expanded response as a function of applied voltage. It is seen that the sensors do not show a detectable response at low voltage, but turn on when the applied voltage exceeds 50 mV. Details of the jump in sensitivity have been described previously.[35] The CVD graphene microribbon sensors show the response to 1,2-dichlorobenzene is 3-4 times higher than that of CNT sensors and 2 times higher than that of CVD graphene sensors. The CVD graphene microribbon sensors also show higher response to toluene molecules compared to CNT based and CVD graphene sensors.

the charge carrier mean free paths are of the order ~20 nm (see Supporting Information) while the ribbons are 2 to 5 μm wide.

Our pristine (monocrystalline) graphene ribbon chemiresistor had a width of 5 μm (see Supporting Information). We observe a negligible sensor response showing that the combination of narrowly spaced edges and a few point defects is insufficient to cause a significant change in the conductance under sensing conditions. In contrast, when the defective (CVD-grown) graphene sensors with existing line defects are cut into microribbons, the chemiresistor response further increases by a factor of 2 to 4 compared to unpatterned CVD-grown graphene chemiresistors, as shown in Figures 2A,B. The sensitivity is enhanced into the parts per billion (ppb) range. Clearly, the combination of edges and line defects enhances the response of the sensor, compared to edges or line defects alone. Further, this experiment proves that in our samples the line defects have a large effect on the response because cutting the graphene into ribbons should only affect the line defects and not the point defects.

Figures 2C,D also compare the response of the graphene ribbon chemiresistors to CNT-based chemiresistors (see Supporting Information). In each case we plot the average response of five different sensors. Notice that the sensor response exceeds that of CNT chemiresistors, suggesting that graphene sensors with edges and line defects offer larger sensitivity to analytes than CNT sensors with point defects alone.

In order to understand the experimental observations described above, we performed calculations of conduction in graphene chemiresistors with and without the presence of line defects and analytes (see Supporting Information). **Figure 3**A shows the distribution of the electric field in a graphene sheet with one hundred 30 nm wide islands containing analytes, as a model for point defects. We assumed the analyte would increase the local resistance of the graphene by 100 times (i.e., significantly more than that one might expect), and did calculations to determine whether there was a significant change in the resistance of the overall device. For the non-defective graphene we used the measured resistivity of our exfoliated graphene, 2.1×10^{-5} Ω·cm. Surprisingly, there was very little effect from point defects. The electric field lines around the point-like defects did not change notably, and there was little change in the overall resistance of the device.

Physically, electrons take the path of lowest resistance in carbon devices,[14] as in other materials. An isolated point defect or other localized chemisorption site does not lead to a significant change in the resistance of the chemiresistor because there is still a low resistance pathway for electron conduction
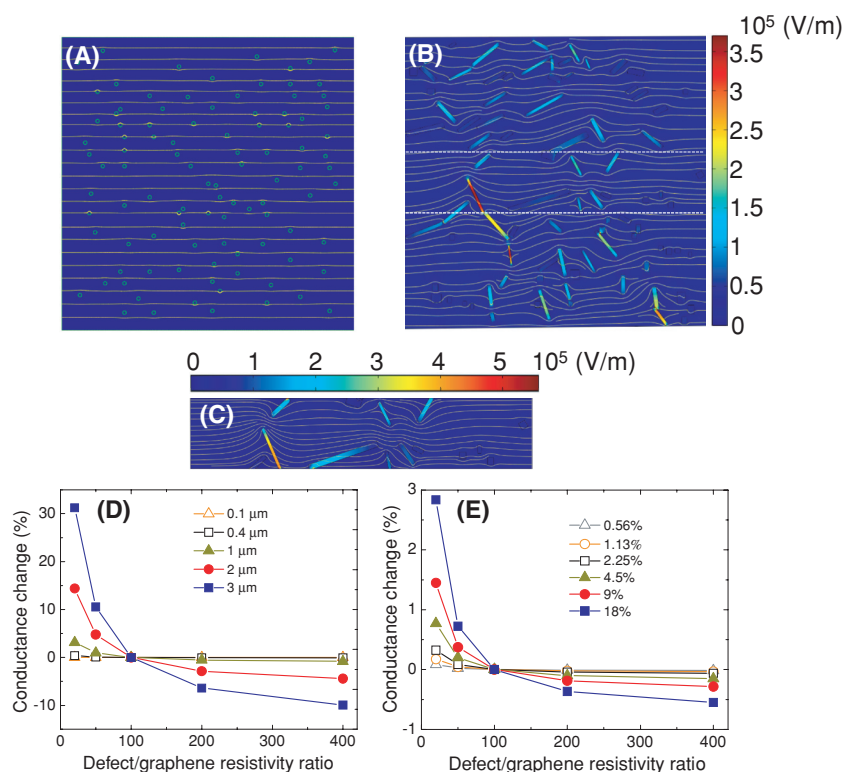

Figure 3. (A) Finite-element simulation of electric field distribution in a 5 μm × 5 μm graphene sample with 100 point defects of 30 nm size, (B) Electric field distribution in a 5 μm × 5 μm graphene sample with line defects that mimic the topography measurement by AFM of an actual graphene sensor in Figure 1B, and, (C) A 1 μm × 5 μm graphene ribbon with randomly distributed line defects. This graphene ribbon is the portion of the sample between the dotted lines in (B). The graphene resistivity is 2.1×10^{-5} Ω·cm and the defect resistivity is 100 times higher. The color bar shows the electric field strength (max: 3.37×10^5 V/m), whereas the streamlines indicate the current density (see Supporting Information for additional information). (D-E) Show the numerical modulation of the chemiresistor conductance when the resistivity ratio of defects to pristine graphene changes from 20×, 50×, 100×, 200×, and 400×. The baseline conductance is chosen at 100×. In (D), the line defect widths are constant at 0.1 μm and the lengths were increased from 0.1 to 3 μm (0.12 to 3.6% of the area). In (E), the point defect concentration (per area) increased from 0.56%, 1.1%, 2.2%, 4.5% 9%, and 18%. We clearly observed that even at a relatively high concentration, the effect of point defects on the conductance change (%) is very small (only 3% change for a defect concentration of 18%), while the effect of line defects are significant (32% change for 3 μm defect length, 3.6% of area).

in analyte-free regions of the graphene. In effect, the low resistance pathways short-circuit the analyte. As a result, according to our calculations, a localized change in the graphene resistance due to adsorption of an analyte will not have a significant effect on the chemiresistor response unless the analyte concentration is very high. This explains why pristine graphene (i.e., monocrystalline and without defects) is less sensitive to analytes.

On the other hand, line defects such as those observed by previous investigators [15,26–28] could have a much stronger effect on the resistance of graphene. Figure 3B shows a simulation of the effect of line defects on the current flow through the chemiresistor. The defect geometry is similar to that observed by AFM (Figure 1B) (see Supporting Information). Notice that, according to the calculations, the presence of line defects or a closely spaced line of point defects greatly perturbs the electric fields and conduction through the chemiresistor. Line defects are needed because graphene is a two-dimensional conductor.

COMMUNICATION

In such a case, the pathways around the line defects are long enough to be difficult to short circuit. The effects of line defects are more pronounced in a graphene ribbon sample (Figure 3C), when the length of the line defects are comparable to the sample width. One would expect that the adsorption of chemical vapors on low-energy sorption sites of line defects should have an important effect on the resistance of the chemiresistor. In a previous study,[29] we found that the concentration of analytes tested here was about 6000 times higher on point defects than on the pristine region of carbon nanotubes. We would expect a similar concentration enhancement on line defects. This high concentration of adsorbed molecules can induce large interactions locally.[30] While our Raman analysis indicates our CVD growth of graphene results in some percentage of bilayer regions, $(2 > I_{2D}/I_G > 1)$,[31] the change of the conductance originated by the electric field from adsorbed molecules will affect the sensitivity of both monolayer and bilayer films because the screening length perpendicular to the graphene plane is greater than the monolayer thickness, or about 0.6 nm.[32]

The results in Figures 3A–C provide the basis for our understanding of the graphene chemiresistor response. We used a simplified model to explore the effects of defect geometry on the sensitivity of the chemiresistors (see Supporting Information). In Figures 3D,E we vary the resistivity ratio between defects and pristine graphene, indicative of the modulation of defect sites upon exposure to analyte molecules. We then compute the change in resistivity ratio (%), and choose the baseline resistivity ratio at 100×. Point defects are randomly distributed to account for 0.6 to 18% of the graphene area. We also changed the length of the line defects from 0.1 to 3 µm, 0.12% and 3.6% of the graphene area, respectively. Figures 3D,E show a plot of how the conductance of the chemiresistor changes when the resistivity ratio between defects to graphene changes from 20× to 400×, for every geometry. Results clearly indicate that the conductance of graphene is more sensitive to the geometry of the defects rather than their concentration.

According to this simple model, pristine graphene or graphene with low concentrations of randomly distributed point defects are less sensitive to the adsorption of gas, because adsorbed molecules on point defects are easily short circuited given the two-dimensional nature of current flow in graphene. In contrast, line defects are more effective in promoting chemiresistor response. We note a more rigorous modeling approach would take into account the carrier concentrations, potential (field) profile, and band structure modification by adsorbates self consistently.[33] However we believe that the simple model presented here contains the more salient features of the physical response. Future work with three-terminal chemFETs will also allow for more detailed modeling and a better understanding of the carrier density distributions controlled by the gate terminal.

Our results suggest that the response of graphene chemiresistors depends on the types and geometry of their defects. Nearly pristine graphene chemiresistors are less sensitive to analyte molecules because adsorbates bind to point defects,[26] which have low resistance pathways around them. As a result, adsorption at point defects only has a small effect on the overall resistance of the device. On the other hand, micrometer-sized line defects or continuous lines of point defects are different

because no easy conduction paths exist around such defects, so the resistance change after adsorption is significant. We also conclude that the two-dimensional nature of defective, CVD-grown graphene chemiresistors causes them to behave differently than CNT chemiresistors. Moreover, this sensitivity is further improved by cutting the graphene into ribbons of width comparable to the line defect dimensions (micrometers in this study). Thus, graphene ribbons with line defects appear to offer superior performance as graphene sensors. Future work to engineer line defects and edges could further enhance the graphene chemiresistor sensitivity.

Experimental Section

Details of fabrication procedures for mechanically exfoliated graphene, CVD graphene sensors, and single-walled carbon nanotube sensors are explained in the Supporting Information. Sensors were then placed in a custom-built PEEK (polyaryletheretherketone) flow cell, and a fused silica passivated capillary was used to connect to a gas chromatograph (GC) inlet. An Agilent 6893N GC/FID-MS with 7683B auto-sampler with a pulse of 100 ms was used to deliver target gas molecules to the sensors at a pressure of 3.6 psi for all experiments. Ultrapure helium was used as a carrier gas at a fixed flow rate. A VoltaLab 10 potentiostat (PGZ100) was used to monitor the change in potential on the sensors upon exposure to trace gas vapors.[34]

Supporting Information

Supporting Information is available from the Wiley Online Library or from the author.

Acknowledgements

[1] M. J. Allen, V. C. Tung, R. B. Kaner, *Chem. Rev.* **2010**, *110*, 132.
[2] S. Das, S. Adam, E. H. Hwang, E. Rossi, *Rev. Modern Phys.* **2011**, *83*, 407.
[3] K. S. Novoselov, A. K. Geim, S. V. Morozov, D. Jiang, M. I. Katsnelson, I. V. Grigorieva, S. V. Dubonos, A. A. Firsov, *Nature* **2005**, *438*, 197.
[4] A. K. Geim, K. S. Novoselov, *Nat. Mater.* **2007**, *6*, 183.
[5] K. I. Bolotin, K. J. Sikes, Z. Jiang, M. Klima, G. Fudenberg, J. Hone, P. Kim, H. L. Stormer, *Solid State Commun.* **2008**, *146*, 351.
[6] A. K. Geim, *Science* **2009**, *324*, 1530.
[7] Y. Dan, Y. Lu, N. J. Kybert, Z. Luo, A. T. C. Johnson, *Nano Lett.* **2009**, *9*, 1472.
[8] J. T. Robinson, F. K. Perkins, E. S. Snow, Z. Wei, P. E. Sheehan, *Nano Lett.* **2008**, *8*, 3137.

[9] R. K. Joshi, H. Gomez, F. Alvi, A. Kumar, *J. Phys. Chem. C* **2010**, *114*, 6610.

[10] L. Ye, B. R. Goldsmith, N. J. Kybert, A. T. C. Johnson, *Appl. Phys. Lett.* **2010**, *97*, 083107.

[11] F. Schedin, A. K. Geim, S. V. Morozov, E. W. Hill, P. Blake, M. I. Katsnelson, K. S. Novoselov, *Nat. Mater.* **2007**, *6*, 652.

[12] N. Govind, J. Andzelm, A. Maiti, *IEEE Sensors J.* **2008**, *8*, 837.

[13] J. A. Robinson, E. S. Snow, S. C. Badescu, T. L. Reinecke, F. K. Perkins, *Nano Lett.* **2006**, *6*, 1747.

[14] A. Salehi-Khojin, F. Khalili-Araghi, M. Kuroda, K. Y. Lin, Jean-Pierre Leburton, R. I. Masel, *ACS Nano* **2010**, *5*, 153.

[15] P. Y. Huang, C. S. Ruiz-Vargas, A. M. van der Zande, W. S. Whitney, M. P. Levendorf, J. W. Kevek, S. Garg, J. S. Alden, C. J. Hustedt, Y. Zhu, J. Park, P. L. McEuen, D. A. Muller, *Nature* **2011**, *469*, 389.

[16] J. Koepke, D. Estrada, J. D. Wood, E. Pop, J. W. Lyding, "Scanning tunneling microscopy study of grain boundaries in graphene grown by chemical vapor deposition on copper foil", presented at *Am. Phys. Soc. March Meeting*, **2011**.

[17] Q. Yu, L. A. Jauregui, W. Wu, R. Colby, J. Tian, Z. Su, H. Cao, Z. Liu, D. Pandey, D. Wei, T. F. Chung, P. Peng, N. P. Guisinger, E. A. Stach, J. Bao, S.-S. Pei, Y. P. Chen, *Nat. Mater.* **2011**, *10*, 443.

[18] J. D. Wood, S. W. Schmucker, A. S. Lyons, E. Pop, J. W. Lyding, *Nano Lett.* **2011**, *11*, 4547.

[19] S. Bhaviripudi, X. Jia, M. S. Dresselhaus, J. Kong, *Nano Lett.* **2010**, *10*, 4128.

[20] X. Li, W. Cai, J. An, S. Kim, J. Nah, D. Yang, R. Piner, A. Velamakanni, I. Jung, E. Tutuc, S. K. Banerjee, L. Colombo, R. S. Ruoff, *Science* **2009**, *324*, 1312.

[21] L. M. Malard, M. A. Pimenta, G. Dresselhaus, M. S. Dresselhaus, *Phys. Rep.* **2009**, *473*, 51.

[22] L. G. Cancado, K. Takai, T. Enoki, M. Endo, Y. A. Kim, H. Mizusaki, A. Jorio, L. N. Coelho, R. Magalhaes-Paniago, M. A. Pimenta, *Appl. Phys. Lett.* **2006**, *88*, 163106.

[23] A. Jorio, M. Dresselhaus, R. Saito, G. F. Dresselhaus, *Raman Spectroscopy in Graphene Related Systems*, Wiley-VCH, Weinheim, Germany **2011**.

[24] Z. Ni, J. P. Jerrell, K. R. Cadwallader, R. I. Masel, *Anal. Chem.* **2007**, *79*, 1290.

[25] M. Ishigami, J. H. Chen, W. G. Cullen, M. S. Fuhrer, E. D. Williams, *Nano Lett.* **2007**, *7*, 1643.

[26] J. An, E. Voelkl, J. W. Suk, X. Li, C. W. Magnuson, L. Fu, P. Tiemeijer, M. Bischoff, B. Freitag, E. Popova, R. S. Ruoff, *ACS Nano* **2011**, *5*, 2433.

[27] J. Lahiri, Y. Lin, P. Bozkurt, I. I. Oleynik, M. Batzill, *Nat. Nanotechnol.* **2010**, *5*, 326.

[28] Y. Liu, B. I. Yakobson, *Nano Lett.* **2010**, *10*, 2178.

[29] A. Salehi-Khojin, K. Y. Lin, R. I. Masel, "The role of defects on the performance of nanotube chemiresistors", presented at *Proc. IEEE Sensors* **2010**, 2620 (DOI: 10.1109/ICSENS.2010.5690217).

[30] E. S. Snow, F. K. Perkins, E. J. Houser, S. C. Badescu, T. L. Reinecke, *Science* **2005**, *307*, 1942.

[31] A. C. Ferrari, J. C. Meyer, V. Scardaci, C. Casiraghi, M. Lazzeri, F. Mauri, S. Piscanec, D. Jiang, K. S. Novoselov, S. Roth, A. K. Geim, *Phys. Rev. Lett.* **2006**, *97*, 187401.

[32] K. T. Lam, D. Seah, S. K. Chin, S. Bala Kumar, G. Samudra, Y. C. Yeo, G. Liang, *IEEE Electron Device Lett.* **2010**, *31*, 555.

[33] J. P. Robinson, H. Schomerus, L. Oroszlany, V. I. Fal'ko, *Phys. Rev. Lett.* **2008**, *101*, 196803.

[34] A. Salehi-Khojin, K. Y. Lin, C. R. Field, R. I. Masel, *Science* **2011**, *329*, 1327.

[35] A. Salehi-Khojin, C. R. Field, J. Yeom, M. A. Shannon, R. I. Masel, *Appl. Phys. Lett.* **2010**, *96*, 163110.

ADVANCED MATERIALS

Supporting Information

Polycrystalline Graphene Ribbons as Chemiresistors

Amin Salehi-Khojin, David Estrada, Kevin Y. Lin, Myung-Ho Bae, Feng Xiong,

Eric Pop, and Richard I. Masel*

Supplementary Materials

Polycrystalline Graphene Ribbons as Chemiresistors

Amin Salehi-Khojin[1,5], David Estrada[2,3], Kevin Y. Lin[1], Myung Ho Bae[2,3], Feng Xiong[2,3], Eric Pop[2,3,4], Richard I Masel[5,*]

[1]Department of Chemical and Biomolecular Engineering,
[2]Department of Electrical and Computer Engineering,
[3]Micro and Nanotechnology Lab,
[4]Beckman Institute
University Of Illinois at Urbana Champaign, USA.
[5]Dioxide Materials
60 Hazelwood Dr
Champaign IL 61820

[*]Corresponding author. E-mail: rich.masel@dioxidematerials.com.

This section contains:
1. **Fabrication and Characterization of Exfoliated Graphene Sensor**
2. **Fabrication Procedure and Raman Characterization of CVD Graphene Sensors**
3. **Mobility and Mean Free Path Estimate in Exfoliated and CVD Graphene Devices**
4. **Fabrication procedure, SEM Image and Raman Spectrum of Single Walled Carbon Nanotube (SWNT) Sensors**
5. **Typical Responses of Carbon Nanotube Sensors**
6. **Typical AFM Topography Profile of CVD Graphene**
7. **COMSOL Simulation Procedure and Simulation of Graphene Sheets with Point and Random Defects**
8. **X-Ray Photoelectron Spectroscopy (XPS) of CVD Graphene**

1. Fabrication and Characterization of Exfoliated Graphene Sensor

Graphene was deposited by mechanical exfoliation from natural graphite with adhesive tape onto a thermally oxidized Si substrate with 100 nm thick SiO_2.[1] The substrate was annealed at 400 $^\circ$C for 35 minutes in Ar/H_2 mixture in a furnace to remove glue residue.[2] The number of the graphene layers was confirmed by optical contrast and Raman spectroscopy.[3] To define source and drain metal electrodes on the graphene sheet, we deposit 40 nm thick Pd with an adhesive layer of 0.5 nm Cr on the graphene by using electron beam (e-beam) lithography, e-beam evaporation and lift-off processes. One more e-beam lithography step was used to form a 5 μm wide graphene channel, followed by an oxygen plasma etch.

(A)

(B)

(C)

(D)

Figure S1. Characterization of exfoliated graphene sensors. (A) Optical image of the device used in this study, (B) typical AFM phase image of an exfoliated graphene device, (C) room temperature resistance vs. gate voltage (R-V_{GD}) characteristics for the device in Fig. S1A (measured in vacuum at $\approx 10^{-5}$ Torr), (D) resistivity of the device in Fig. S1A, calculated from the measured 4 pt resistance. The red dots indicate the corresponding resistance value for the two terminal measurement performed in air prior to chemical sensing measurements.

2. Fabrication Procedure and Raman Characterization of CVD Graphene Sensors

Cr (10 nm)/Au (100 nm) electrodes were first patterned onto Si/SiO_2 substrates using standard lithographic techniques. Graphene films were grown using an Etamota chemical vapor deposition (CVD) system, on 1.4 mil copper foils purchased from Basic Copper. The foils were annealed under Ar/H_2 flow for 45 minutes and graphene was grown under a $CH_4/H_2/Ar$ flow (17:1:3 ratio) at 1000 °C for 30 min.[4] The resulting Cu/graphene substrates are cooled to room temperature under the same gas flow at a rate of ~20 °C/min. Graphene is subsequently transferred to the sensor electrodes by coating the graphene with PMMA, removing the backside graphene in an O_2 plasma, and then etching the backside copper in a 1M $FeCl_3$ solution. PMMA is then removed in a 1:1 solution of Methlyene Chloride:Methanol and sensors are held at 400 °C for 35 minutes in Ar/H_2 mixture in a CVD furnace to remove residues. Extended graphene films, i.e. the graphene covers the entire sensor area (≈6,000 μm^2) and micro-ribbons are defined with standard photolithography using a bilayer of PMGI and Shipley 1813 resists. Graphene is patterned by O_2 plasma etching. Photoresist and PMGI are then removed in Remover PG and sensors again held at 400 °C for 35 minutes in Ar/H_2 mixture in a CVD furnace to remove residues.[2, 5] Raman spectra were collected using a Renishaw confocal microscope with 633 nm excitation laser and spot size ~1 μm, and analyzed to quantify graphene layer numbers[4] and estimate crystallite size.[6, 7] We then measured the resistance of all of the sensors, and selected the ones with low resistance. The measured resistance was between 60 and 70 Ohms for all but one of the samples. The sheet resistance of the graphene was measured using a HL5500PC Hall Effect Measurement System in a Van der Pauw configuration. We find the sheet resistance of our ungated (as-deposited) CVD graphene is ~8850 $\Omega/\square$. Given the geometry of our sensors (W = 1 mm, L ~ 7 μm) we expect the graphene sensor to have an average channel resistance of ~62 Ω with contact resistance $2R_C < 8\ \Omega$ (some of which is due to metal leads).

(A)   (B)   (C)
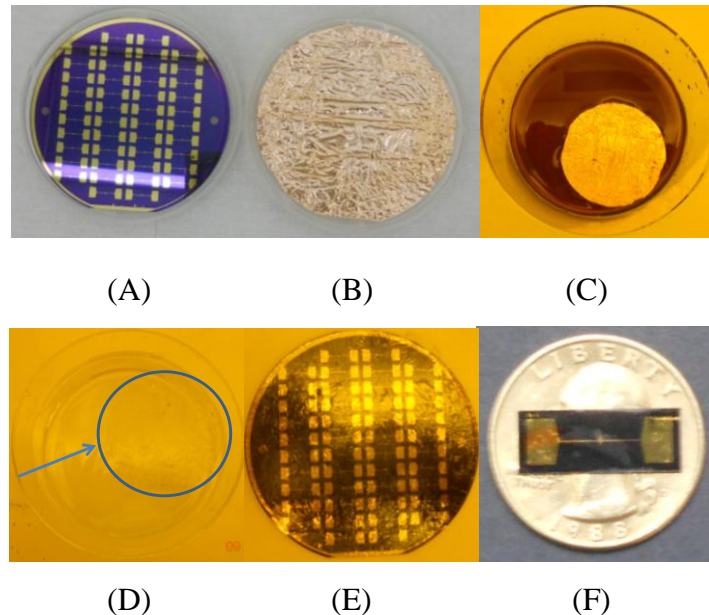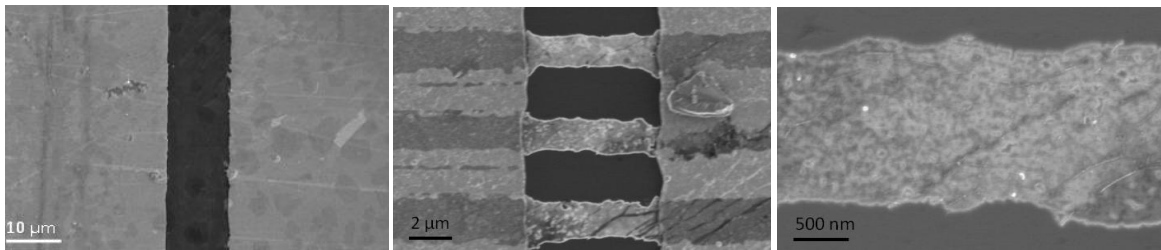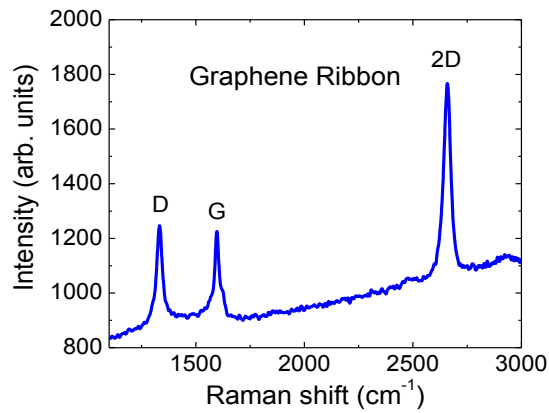
(D)   (E)   (F)

Figure S2. Fabrication procedure of wafer scale graphene sensors. (A) Cr/Au Patterned Electrodes, (B) 100 mm Copper foil with CVD grown Graphene, (C) PMMA/Graphene/Copper foil in $FeCl_3$, (D) PMMA/Graphene in deionized water after etching, (E) Sensor electrodes with PMMA/Graphene film after transfer, and (F) Sensor with transferred and patterned graphene.
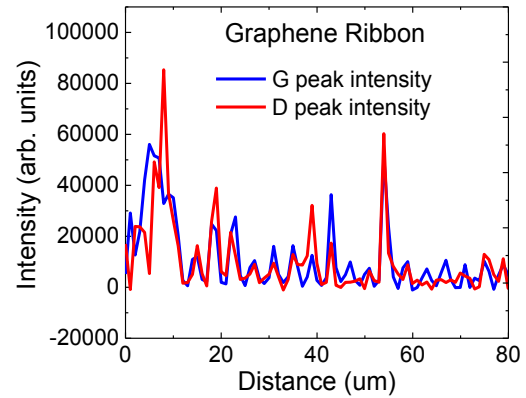
(A) (B) (C)

(D) (E)

Figure S3. (A) Zoom-in SEM image of extended graphene sensor (middle channel) and two electrodes (sides), (B) SEM images of graphene ribbon sensors, (C) Zoom-in SEM image of single ribbon, (D) Raman spectrum of graphene ribbon, and (E) typical line scan results for the G and D peak intensities for graphene ribbon sensor.

4

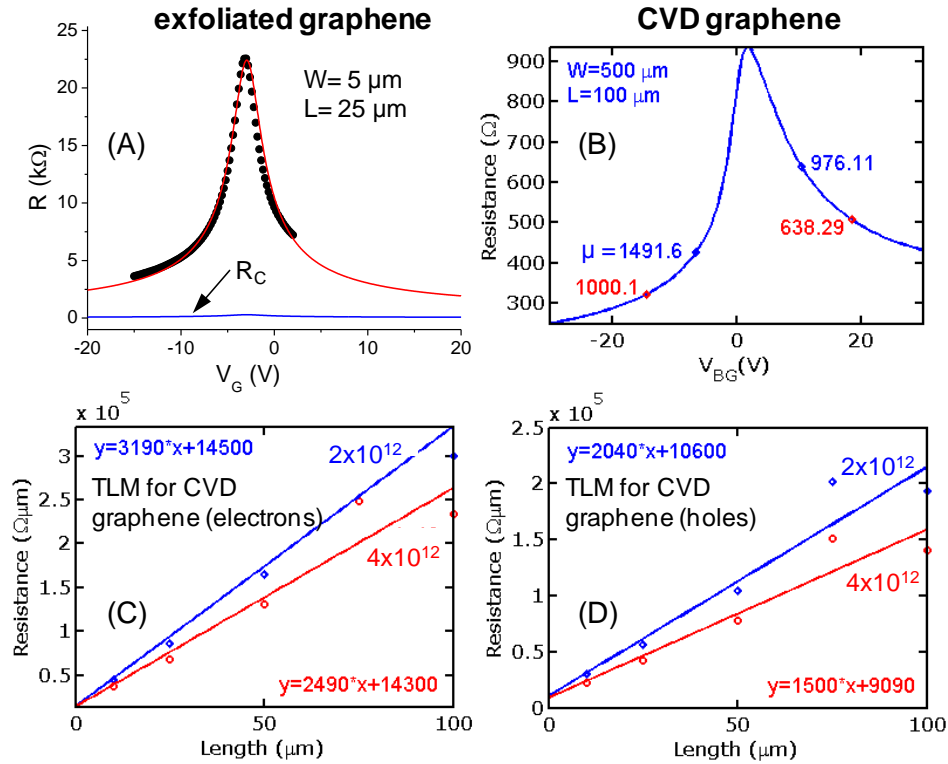## 3. Mobility and Mean Free Path Estimate in Exfoliated and CVD Graphene Devices

Figure S4. **(A)** R-V_{GS} characteristics and curve fitting[8] for exfoliated ("pristine") graphene sample (L = 25, W = 5 μm) with μ ~ 4500 cm^2/V·s and R_C ~ 2 kΩ·μm per contact (slightly dependent on gate voltage). **(B)** CVD-grown graphene (L = 100 μm and W = 500 μm). Best fit mobility indicated on the curve, e.g. $μ_p$ ~ 1000 cm^2/V·s at p = $4×10^{12}$ cm^{-2} hole density, or $μ_n$ ~ 976 cm^2/V·s at $2×10^{12}$ cm^{-2} electron density. **(C-D)** Transfer length method (TLM) estimate of contact resistance to CVD graphene for samples of varying length. Contact resistance is R_C ~ 7 kΩ·μm for electrons and ~ 5 kΩ·μm for holes, per contact, slightly dependent on gate voltage. The results are consistent with our estimates for CVD graphene in Section 2 (e.g. R_C ~ 5-7 Ω for one contact of 1 mm width). In all cases data are symbols and fits are solid lines.

The carrier mean free path can be estimated by using a semiclassical relation between the mobility and the mean free path,[9] $l = (h/2q)μ_0(n/π)^{1/2} ≈ 16$ nm, for $n = 2×10^{12}$ cm^{-2} and $μ_0 = 1000$ cm^2/Vs for the CVD grown graphene FET. Here, h is the Planck constant and q is elementary charge. In addition, for the exfoliated graphene, $l ≈ 74$ nm for $n = 2×10^{12}$ cm^{-2} and $μ_0 = 4500$ cm^2/Vs. Therefore, after scattering by an edge of our wide graphene channel (2~5 μm wide), it is highly probable the carriers experience numerous scattering events in the inner region of the ribbon before the next edge scattering event occurs. Consequently, we can neglect the conductance change due to the adsorbed molecules at the edges of the graphene channel.

4. Fabrication procedure, SEM Image and Raman Spectrum of Single Walled Carbon Nanotube (SWNT) Sensors

A commercially available SWNT solution was obtained from NanoIntegris. The SWNT solution was then diluted to desired concentration in 25 mL solution of 1% weight/volume (w/v) sodium dodecyl sulfate (SDS) in water before being vacuum filtrated with mixed cellulose ester (MCE) membranes (Millipore, 0.22 micron pore size). After the SWNTs were successfully deposited onto the membranes, the wet MCE-SWNT membrane was dried for at least 2 hours under 15 in-Hg gauge pressure before multiple rinsing with approximately 80 mL of purified and deionized water (Millipore, MilliQ water). Multiple rinsing was intended to completely remove the SDS residue from the MCE-SWNT membrane. Finally, a stamp technique was used to transfer homogeneous, randomly aligned CNT films to predefined Cr/Au sensor electrodes (10, 100 nm).[10-12]
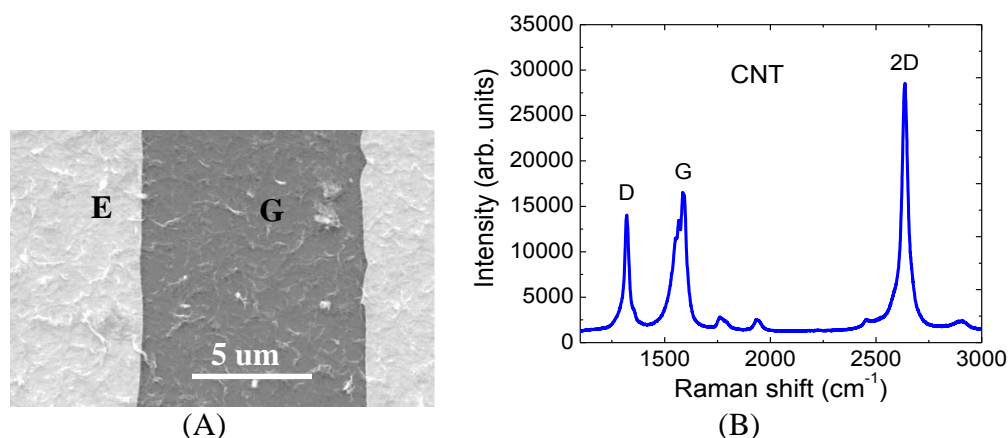
(A)   (B)

Figure S5. (A) SEM image of carbon nanotube sensor, and (B) Raman spectrum of carbon nanotube film. The gap zone and electrodes are labeled (G) and (E) in the SEM image, respectively.
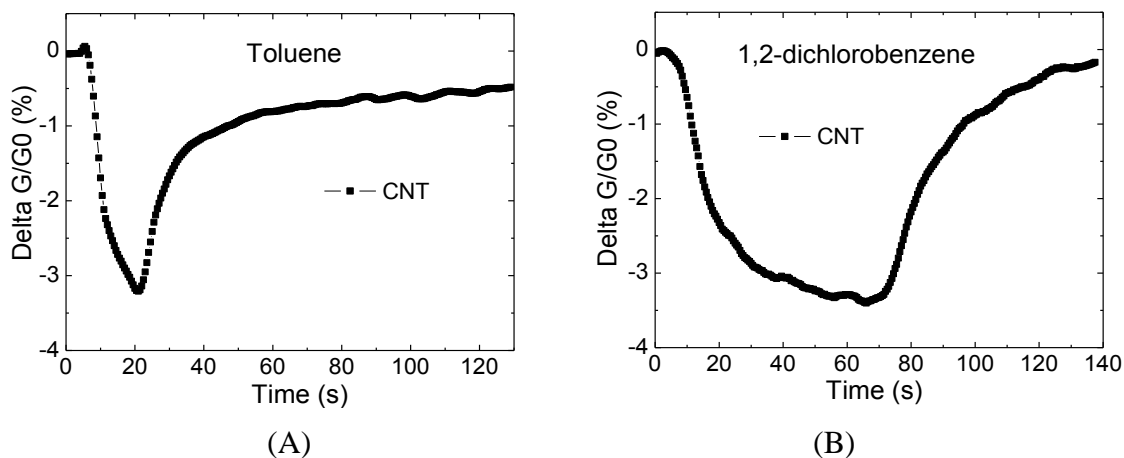
5. Typical Responses of Carbon Nanotube Sensors

(A)   (B)

Figure S6. Typical responses of CNT sensors to 10^{14} molecules of toluene and 10^{15} molecules of 1,2-dichlorobenzene, respectively.

6. Typical AFM Topography Profile of CVD Graphene

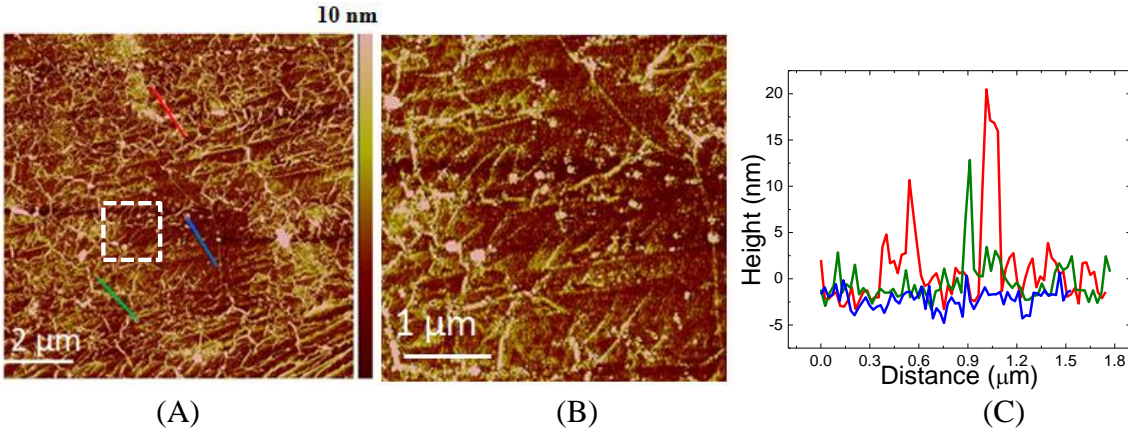|		
(A)	(B)	(C)

Figure S7. (A) an AFM image of the CVD based extended graphene. The white dashed box shows the (B) close view of AFM image for CVD based extended graphene, and (C) Profile of topography along three red, blue and green lines in Fig. (S7.A)

7. COMSOL Simulation Procedure and Simulation of Graphene Sheets with Point and Random Defects

We used *COMSOL Multiphysics* to build a two-dimensional finite element model seeking to understand how electric fields change near point and line defects. The modeled graphene chemiresistors have dimensions of 5 x 5 μm^2 and 1 x 5 μm^2 (for the ribbon device), with a resistivity of 2.1×10^{-5} $\Omega \cdot cm$ as measured in our exfoliated graphene sensors. A fixed potential (0.1 V) is applied to the left boundary of the chemiresistor while plotting out the steady state electric field distribution. Figure S8 shows the results for a random distribution of point defects. Figure S9 shows the results for well-aligned linear defects.
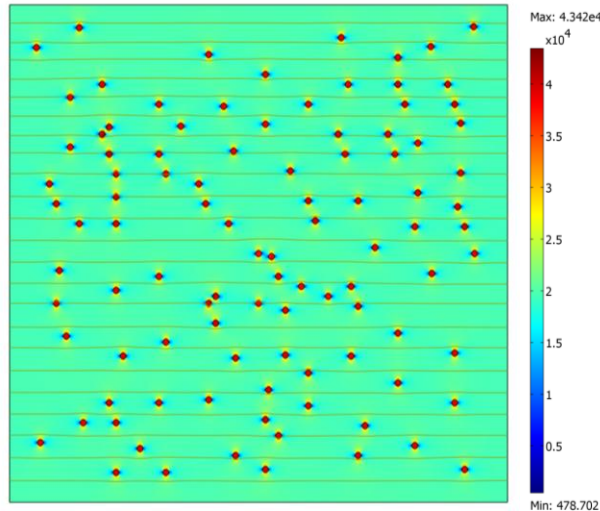

Figure S8. COMSOL simulation of electric field distribution in extended graphene of size 5 μm $\times$ 5 μm with 100 point defects of 30 nm size. This is the same result as shown in Figure 3A in the main text, but plotted in a different color bar scale to better illustrate the electric field distribution. Here the max is 4.32×10^4 V/m.
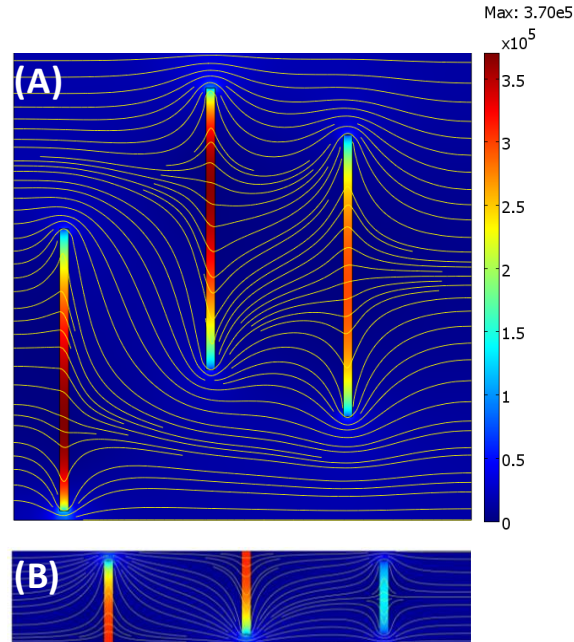
Figure S9. Results of a finite-element simulation of the electric field distribution in a (A) 5×5 μm^2 graphene with 3 line defects of 0.1×3 μm^2, and, (B) 1×5 μm^2 graphene ribbon with two line defects of 0.1×0.9 μm^2 and a third of 0.1×0.8 μm^2. The graphene resistivity is 2.1×10^{-5} Ω·cm and defect resistivity is 100 times higher. The color bar shows the electric field strength (max: 3.37 × 10^5 V/m), whereas the streamlines indicate the current density.
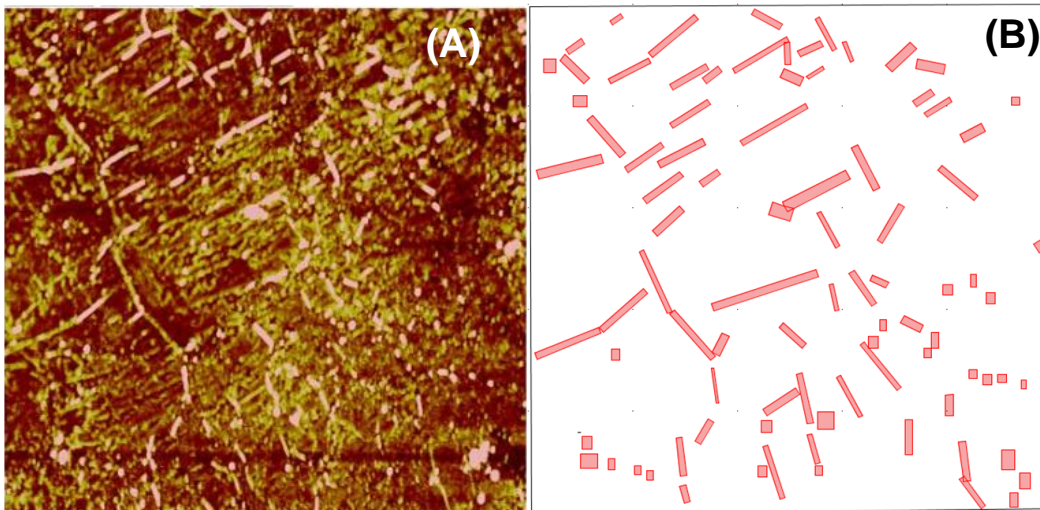

Figure S10. Side-by-side comparison of (A) the topography measurement by AFM of an actual graphene sample (5× 5 μm^2 scan, Fig. 1B in the manuscript), and (B) the defect distribution used for the simulation results shown in Fig. 3B.

8

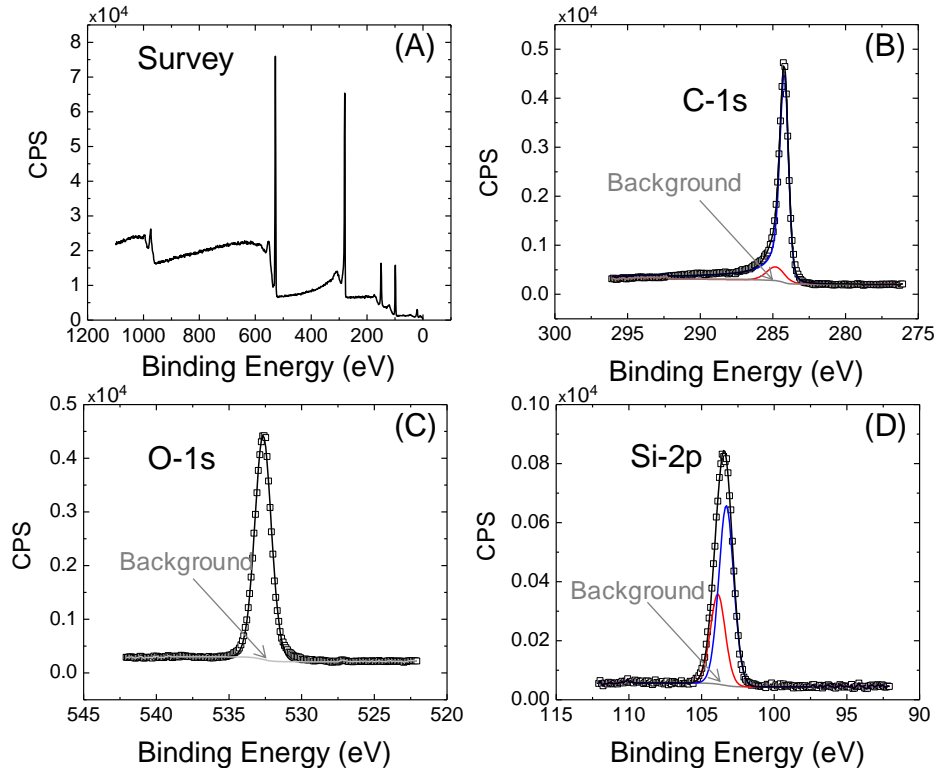## 8. X-Ray Photoelectron Spectroscopy (XPS) of CVD Graphene

Figure S11. Typical XPS results of counts per second (CPS) vs. Binding Energy for our graphene samples grown via CVD and transferred to SiO$_2$/Si substrates; **(A)** survey, **(B)** C-1s, **(C)** O-1s, and **(D)** Si-2p peaks. The lack of a peak at ≈ 290 eV indicates the lack of PMMA residues in our samples after processing.[13] In (B-D) open squares are raw data and solid lines are fits.

Using the procedures described in Section 2, we prepared a large scale CVD graphene film supported by a SiO$_2$/Si substrate for XPS. XPS is accomplished using a KRATOS Axis Ultra 165 mm X-ray photoelectron spectrometer, and conducted at 3 different locations of our millimeter scale film. Results indicate our CVD graphene is relatively clean, i.e. there are no PMMA residues as evidenced by the lack of a peak in the counts per second (CPS) vs. Binding Energy spectrum near the C-1S peak at ≈ 290 eV.[13] We also do not see evidence of a C-O bond in the C-1s peak. This is confirmed by the lack of peaks above the adventitious hydrocarbon peak at 284.6 eV, and by the single O-1s peak near 582 eV.[13] The intensity of the graphene peak was determined by fitting the C-1s region collected at an electron emission angle of 0° using a Shirley background and a Doniach-Sunjic line-shape for graphene based upon fitting the C-1s of highly ordered pyrolytic graphite.[14]

REFERENCES AND NOTES

[1]   K. S. Novoselov, A. K. Geim, S. V. Morozov, D. Jiang, Y. Zhang, S. V. Dubonos, I. V. Grigorieva, A. A. Firsov, *Science* **2004**, *306*, 666.

[2]   M. Ishigami, J. H. Chen, W. G. Cullen, M. S. Fuhrer, E. D. Williams, *Nano Letters* **2007**, *7*, 1643.

[3]   A. C. Ferrari, J. C. Meyer, V. Scardaci, C. Casiraghi, M. Lazzeri, F. Mauri, S. Piscanec, D. Jiang, K. S. Novoselov, S. Roth, A. K. Geim, *Physical Review Letters* **2006**, *97*, 187401.

[4]   X. Li, W. Cai, J. An, S. Kim, J. Nah, D. Yang, R. Piner, A. Velamakanni, I. Jung, E. Tutuc, S. K. Banerjee, L. Colombo, R. S. Ruoff, *Science* **2009**, *324*, 1312.

[5]   Y. Dan, Y. Lu, N. J. Kybert, Z. Luo, A. T. C. Johnson, *Nano Letters* **2009**, *9*, 1472.

[6]   L. G. Cancado, K. Takai, T. Enoki, M. Endo, Y. A. Kim, H. Mizusaki, A. Jorio, L. N. Coelho, R. Magalhaes-Paniago, M. A. Pimenta, *Applied Physics Letters* **2006**, *88*, 163106.

[7]   A. Jorio, M. Dresselhaus, R. Saito, G. F. Dresselhaus, *Raman Spectroscopy in Graphene Related Systems*, Wiley-VCH, Weinheim, Germany **2011**.

[8]   V. E. Dorgan, M. H. Bae, E. Pop, *Applied Physics Letters* **2010**, *97*, 082112.

[9]   E. H. Hwang, S. Adam, S. Das Sarma, *Physical Review Letters* **2007**, *98*, 186806.

[10]   A. Salehi-Khojin, C. R. Field, J. Yeom, M. A. Shannon, R. I. Masel, *Applied Physics Letters* **2010**, *96*, 163110.

[11]   A. Salehi-Khojin, F. Khalili-Araghi, M. Kuroda, K. Y. Lin, Jean-Pierre Leburton, R. I. Masel, *ACS Nano* **2010**, *5*, 153.

[12]   A. Salehi-Khojin, K. Y. Lin, C. R. Field, R. I. Masel, *Science* **2011**, *329*, 1327.

[13]   G. Beamson, D. Briggs, *High resolution XPS of organic polymers*, John Wiley & Sons, **1997**.

[14]   S. Unarunotai, J. Koepke, C.-L. Tsai, F. Du, C. E. Chialvo, Y. Murata, R. Haasch, I. Petrov, N. Mason, M. Shim, J. Lyding, J. A. Rogers, *ACS Nano* **2010**, *4*, 5591.